Letter | Editors' Suggestion

Ground state of $Ce_3Bi_4Pd_3$ unraveled by hydrostatic pressure

M. O. Ajeesh,[1] S. M. Thomas,[1] S. K. Kushwaha,[2] E. D. Bauer,[1] F. Ronning,[1] J. D. Thompson,[1] N. Harrison,[2] and P. F. S. Rosa[1]

[1]*Los Alamos National Laboratory, Los Alamos, New Mexico 87545, USA*

[2]*National High Magnetic Field Laboratory, Los Alamos, New Mexico 87545, USA*

(Received 18 October 2021; revised 4 February 2022; accepted 23 September 2022; published 10 October 2022)

Noncentrosymmetric $Ce_3Bi_4Pd_3$ has attracted a lot of attention as a candidate for strongly correlated topological material, yet its experimental ground state remains a matter of contention. Two conflicting scenarios have emerged from a comparison to the prototypical Kondo insulator $Ce_3Bi_4Pt_3$: Either $Ce_3Bi_4Pd_3$ is a spin-orbit-driven topological semimetal or a Kondo insulator with smaller Kondo coupling than its Pt counterpart. Here, we determine the ground state of $Ce_3Bi_4Pd_3$ via electrical resistivity measurements under hydrostatic pressure, which is a clean symmetry-preserving tuning parameter that increases hybridization but virtually preserves spin-orbit coupling. $Ce_3Bi_4Pd_3$ becomes more insulating under pressures up to 2.3 GPa, which is a signature of Ce-based Kondo insulating materials in the considered pressure range. Its small zero-pressure gap increases quadratically with pressure, similar to the behavior observed in the series $Ce_3Bi_4(Pt_{1-x}Pd_x)_3$, which indicates that Pt substitution and applied pressure have a similar effect. Our result not only demonstrates that Kondo coupling, rather than spin-orbit coupling, is the main tuning parameter in this class of materials, but it also establishes that $Ce_3Bi_4Pd_3$ has a narrow-gap Kondo insulating ground state.

DOI: 10.1103/PhysRevB.106.L161105

Topological classification schemes have uncovered unprecedented quantum states of matter by employing a bulk invariant to distinguish states that share the same symmetries [1–4]. A prototypical example of a topological state of matter is the fractional quantum Hall state, which exhibits a nonlocal order parameter, fractionalized excitations, and long-range entanglement [5,6]. For three-dimensional insulators, the simplest case of inversion-symmetric bulk materials utilizes the so-called Z_2 topological invariant, which is defined as the product of the parities of the occupied bands at high-symmetry points in momentum space, to determine whether the material is topologically nontrivial [7–9]. A topological insulating state stems from a combination of spin-orbit interactions and time-reversal symmetry, and its edge state is typically a manifestation of gapless excitations at the interface between topologically distinct regions [6,10].

The concept of band topology can also be extended beyond insulating and inversion-symmetric states, which has enabled the discovery of new classes of topological matter [11–15]. In particular, a Weyl-Kondo semimetal (WKSM) phase has recently been predicted to emerge in strongly correlated materials with broken inversion symmetry [16,17]. In a WKSM, the Kondo effect gives rise to strongly renormalized Weyl nodes in the bulk and Fermi arcs on the surface. Notably, the large renormalization factor of nodes pinned to the Fermi energy is predicted to enable thermodynamic quantities, such as specific heat, to experimentally probe Weyl nodes in these materials.

Noncentrosymmetric $Ce_3Bi_4Pd_3$ has been put forward as a prime Weyl-Kondo semimetal candidate [16,18], yet its ground state remains a matter of contention. On one hand, the electronic contribution to the specific heat includes a linear-in-temperature term as well as a ΓT^3 term whose prefactor Γ is consistent with the theoretical WKSM proposal [16,19]. In addition, the weak temperature dependence of electrical resistance reported initially was taken as an indication of the absence of a well-defined energy gap [19]. Furthermore, recent experiments at zero magnetic field reveal a giant spontaneous Hall effect, which is explained as a substantial Berry curvature contribution coming from tilted renormalized Weyl nodes [20]. On the other hand, independent experimental reports argued for a small-gap insulating ground state based on activated behavior in electrical resistivity and Hall resistivity as well as fits of the low-temperature specific heat to a Schotte-Schotte anomaly [21]. In addition, a broad maximum in magnetic susceptibility at about $T_M = 5$ K was attributed to a Kondo gap scale of 15–20 K that can be suppressed with applied magnetic fields.

To shed light on this issue, a comparison to the prototypical Kondo insulator $Ce_3Bi_4Pt_3$ [22–26] is key. According to the WKSM scenario, the reduction in spin-orbit coupling (SOC) promoted by replacing Pt with Pd is the main driver of the destabilization of the Kondo gap in $Ce_3Bi_4Pd_3$ [16,19]. Dzaber *et al.* found that the isovalent substitution series $Ce_3Bi_4(Pt_{1-x}Pd_x)_3$ is also virtually isovolume, which leads to the conclusion that a reduction in Kondo coupling J_K by chemical pressure is not the dominant factor in the series [19]. In the small-gap insulating scenario, however, $Ce_3Bi_4Pd_3$ is a reduced J_K version of $Ce_3Bi_4Pt_3$ even in the absence of chemical pressure effects [21]. As illustrated by band-structure calculations, an explanation for the reduced d-f hybridization strength along the isovolume series is the reduction in radial

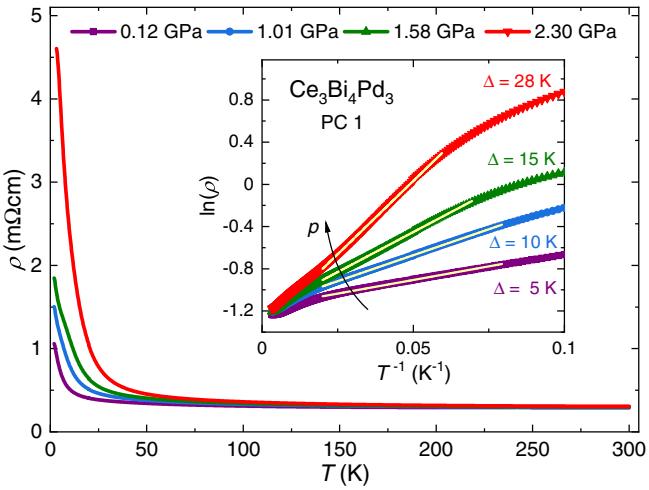

FIG. 1. Electrical resistivity of $Ce_3Bi_4Pd_3$ as a function of temperature at different applied pressures. The inset shows the corresponding Arrhenius plot, $\ln(\rho)$ vs $1/T$, along with linear fits (yellow lines).

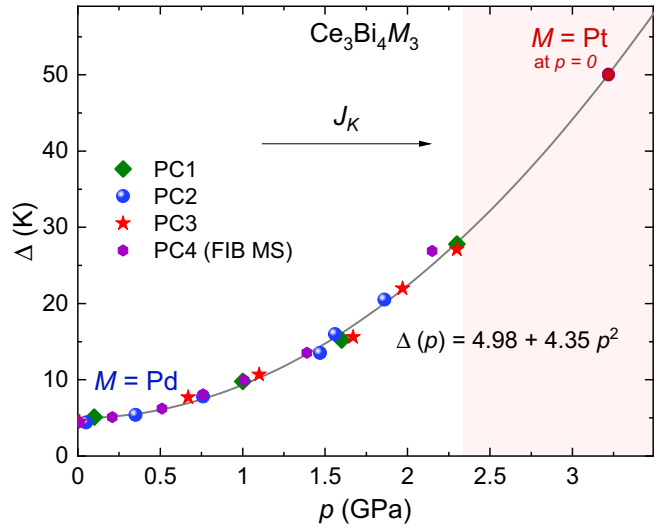

FIG. 2. Activated gap Δ of $Ce_3Bi_4Pd_3$ as a function of applied pressure; extracted from electrical-resistivity measurements on four different samples. The solid line is a quadratic fit to the data. Pressure increases the Kondo coupling J_K and in turn increases the hybridization gap towards that of $Ce_3Bi_4Pt_3$.

extent of the ligand atoms going from 5*d* electrons in Pt to 4*d* electrons in Pd [27].

In this Letter, we employ hydrostatic pressure to unravel the narrow-gap insulating ground state of $Ce_3Bi_4Pd_3$. Here, pressure is an ideal tuning parameter because of its symmetry-preserving nature and ability to increase hybridization while preserving spin-orbit coupling with the advantage of not introducing disorder. Our electrical resistivity measurements show that $Ce_3Bi_4Pd_3$ behaves as a Kondo insulator under pressure: It becomes progressively more insulating as the hybridization increases, and its insulating gap increases quadratically, similar to the behavior in the series $Ce_3Bi_4(Pt_{1-x}Pd_x)_3$.

Figure 1 shows the temperature-dependent electrical resistivity $\rho(T)$ of $Ce_3Bi_4Pd_3$ at different applied pressures. At low pressures, $\rho(T)$ resembles ambient-pressure data previously obtained in samples polished to remove surface contamination [21]. At $p = 0.12$ GPa, $\rho(T)$ increases upon decreasing temperature and exhibits an activated behavior at low temperatures. A fit of the data to an Arrhenius formula, $\rho = \rho_0 \exp(-\Delta/k_B T)$, yields a small activated gap of 5 K, as shown in the inset of Fig. 1.

We note that the magnitude of the extracted gap has to be considered with caution because the temperature range of the fit is limited to between 50 and 12 K, which is higher than the gap magnitude. Such a limited temperature range, however, is also observed in the prototypical Kondo insulator $Ce_3Bi_4Pt_3$ [22–24]. The hybridization-driven gap effectively closes at high temperatures ($T > 2\Delta/k_B$), and the system behaves similar to a Kondo metal. The extraction of an activated gap in $Ce_3Bi_4Pt_3$ is further complicated by its temperature dependence, which is expected within a mean-field approximation to an Anderson lattice model [28]. Furthermore, narrow gaps are typically susceptible to even small amounts of defects and impurities at low temperatures, and electrical resistivity measurements are particularly affected by in-gap states [29]. Although early reports attributed the low-temperature resistivity saturation to parallel conduction by extrinsic impurity states and variable-range hopping, recent many-body calculations highlight the role of disorder on intrinsic carriers through finite lifetimes [30]. In the latter scenario, a scattering-rate-dependent temperature T^* marks the crossover from activated behavior at modest temperature to resistivity saturation at low temperatures. Nonetheless, estimates of the gap in Kondo insulators from quantities that are less dependent on the scattering rate, such as Hall resistivity, magnetic susceptibility, and specific heat, yield similar, albeit slightly larger, gap values, e.g., ≈20 K in $Ce_3Bi_4Pd_3$ at ambient pressure [21]. Therefore, although the magnitude of the extracted gap cannot be taken at face value, its pressure dependence is expected to provide qualitative information about the Kondo physics at play.

In fact, the low-temperature resistivity increases monotonically as a function of pressure, which is the first indication that pressurized $Ce_3Bi_4Pd_3$ becomes more insulating in a continuous manner. Moreover, at the maximum pressure of our measurements, $p = 2.3$ GPa, both the inverse resistance ratio, $\rho_{2\,K}/\rho_{300\,K}$, and the activated gap increase by a factor of 5 compared to the ambient-pressure values. Importantly, Fig. 2 shows that the activated gap increases quadratically with pressure similar to the behavior observed in the substitution series $Ce_3Bi_4(Pt_{1-x}Pd_x)_3$ with the caveat that no gap was reported for $x = 0.37$ [19], which is possibly caused by increased disorder from substitution. The quadratic increase in $\Delta(p)$ is consistent across all the samples measured (see Supplemental Material [31]). Though the slope extracted from the $\ln(\rho)$ vs T^{-1} plot depends on the temperature range of the linear fit, the variation in the magnitude of the energy gap is at most 1%. A quadratic fit to the data (solid line in Fig. 2) provides the pressure dependence of the energy gap as $\Delta(p) = 4.98 + 4.35p^2$. An extrapolation of this trend to higher pressures indicates that an applied pressure of 3.2 GPa would be required to reach the activated gap of the end member $Ce_3Bi_4Pt_3$, $\Delta \approx 50$ K [22]. Similarly, the activated

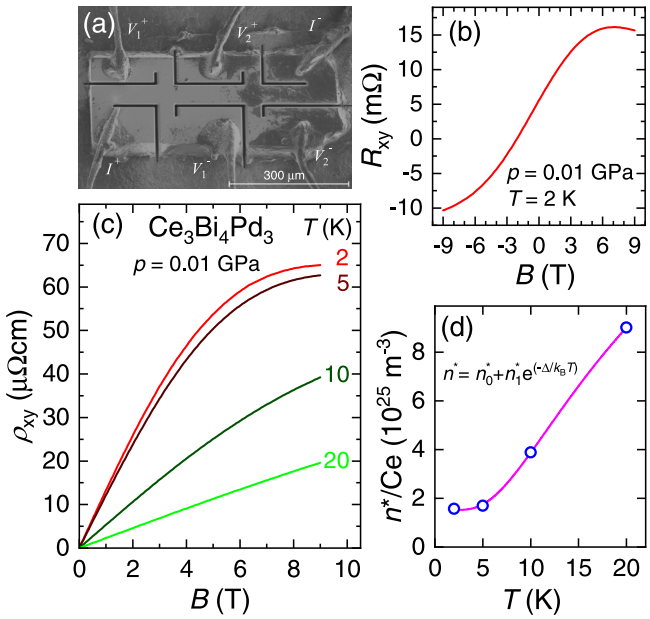

FIG. 3. (a) Scanning electron micrograph of the microstructure device used for Hall resistivity measurements. (b) Hall resistance of $Ce_3Bi_4Pd_3$ at $p = 0.01$ GPa and 2 K measured in positive and negative fields. (c) Magnetic field dependence of Hall resistivity $\rho_{xy}(B)$, obtained by antisymmetrizing the as-measured data, of $Ce_3Bi_4Pd_3$ at $p = 0.01$ GPa and different temperatures. (d) The carrier density $n^* = B/e\rho_{xy}$ as a function of temperature (blue circles). The solid line is a fit to the data as described in the main text.

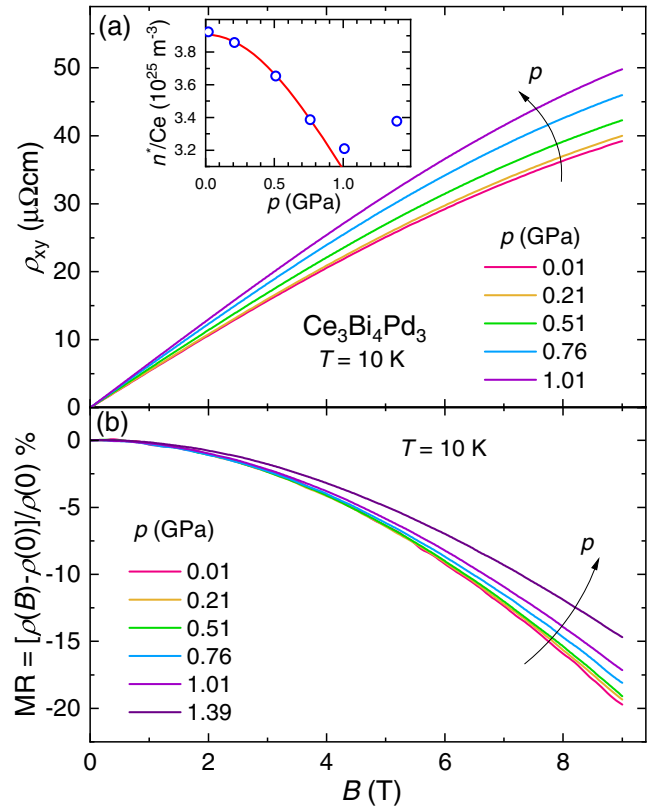

FIG. 4. (a) Hall resistivity of $Ce_3Bi_4Pd_3$ as a function of magnetic fields at $T = 10$ K measured at different pressures. The inset shows the pressure dependence of the carrier density n^* (blue circles) where the red line is the expected curve inferred from the pressure dependence of the activated gap $\Delta(p)$ (see main text). (b) Magnetic field dependence of magnetoresistance $\mathrm{MR}(B) = [\rho(B) - \rho(0)]/\rho(0)$ of $Ce_3Bi_4Pd_3$ measured at $T = 10$ K under different applied pressures.

gap at $p = 2.3$ GPa would correspond to a stoichiometry of $Ce_3Bi_4(Pt_{0.8}Pd_{0.2})_3$.

In order to understand the effect of pressure on the carrier density, we turn to Hall resistivity measurements. We note that magnetotransport properties at low temperatures are found to be sensitive to impurity inclusions and are strongly sample dependent, even after careful polishing. Possible impurity phases include elemental Bi and Bi-Pd binaries of varying stoichiometry that undergo superconducting transitions at low temperatures [32–39]. A detailed discussion of the extrinsic contributions to the magnetotransport is provided in the Supplemental Material [31]. In order to minimize the contributions from the impurity phases and to obtain well-defined Hall geometry, a microstructure device was fabricated on a thin sample ($600 \times 250 \times 50\ \mu\mathrm{m}^3$) of $Ce_3Bi_4Pd_3$ using a focused ion beam. A scanning electron micrograph of the microstructure device is shown in Fig. 3(a). Raw Hall resistance data at $p = 0.01$ GPa and $T = 2$ K are shown in Fig. 3(b). The magnetic field dependence of the Hall resistivity, $\rho_{xy}(B)$, measured at $p = 0.01$ GPa and different temperatures is presented in Fig. 3(c). Here, ρ_{xy} is obtained by antisymmetrizing the resistivity data measured in positive and negative magnetic fields to remove any magnetoresistance contribution from misalignment of the electrical contacts.

At low temperatures, ρ_{xy} increases linearly with magnetic field followed by a downward curvature at higher fields. This is consistent with the results from previous high-field studies which revealed the closing of the Kondo hybridization gap at an applied magnetic field of $B_c \approx 11$ T [21]. The positive $\rho_{xy}(B)$ at low fields indicates that electronic conduction is dominated by holelike carriers. The linear $\rho_{xy}(B)$ at low fields allows for a straightforward estimation of the carrier density from a single-band model, $n^* = 1/eR_H$, where the Hall constant is $R_H = \rho_{xy}/B$. The resulting carrier density, calculated from the slope of $\rho_{xy}(B)$ below 2 T, is plotted as a function of temperature in Fig. 3(d). Because n^* increases with temperature in a thermally activated manner, it is possible to determine the associated energy gap. A fit to the data (solid line) using $n^* = n_0^* + n_1^* \exp(-\Delta/k_B T)$ yields $n_0^* = 1.5 \times 10^{25}\ \mathrm{m}^{-3}$, $n_1^* = 24 \times 10^{25}\ \mathrm{m}^{-3}$, and $\Delta = 23 \pm 1$ K. The obtained values of carrier density and hybridization gap are in excellent agreement with previous reports [20,21].

The evolution of ρ_{xy} vs B, measured at $T = 10$ K, with applied pressure is presented in Fig. 4(a). It is immediately evident that the slope of $\rho_{xy}(B)$ increases with increasing pressure, suggesting a decrease in carrier density. The carrier density, estimated from the slope of $\rho_{xy}(B)$ below 2 T, is plotted in the inset of Fig. 4(a) (circles). Such a decrease in n^* with increasing pressure can be understood as the reduction in thermally accessible carriers due to the enhanced energy gap under applied pressure. To further verify this scenario, we calculate n^* as a function of pressure at constant

temperature using the pressure dependence of the energy gap $\Delta(p)$ extracted from $\rho(T)$ (see Fig. 2). Here, we used the equation for activated behavior $n^* = n_0^* + n_1^* \exp[-\Delta(p)/k_B T]$ along with the pressure dependence of the energy gap $\Delta(p) = 23 + 4.35p^2$ at 10 K. The calculated $n^*(p)$ [solid line in the inset of Fig. 4(a)] is in excellent agreement with the experimental values obtained from $\rho_{xy}(B)$ data to $p = 1$ GPa. We note that the determination of the pressure dependence of n^* at lower temperatures is hindered by the effect of impurity phases. In particular, impurity contributions become increasingly prominent at higher temperatures as pressure increases. Above 1 GPa, it is not possible to estimate the intrinsic carrier density even at $T = 10$ K (see Supplemental Material [31]). Nonetheless, below 1 GPa the mobility of the carriers can be obtained via the ratio R_H/ρ_{xx} evaluated at zero magnetic field. The hole mobility, estimated at $T = 10$ K, decreases from 104.4 $\mathrm{cm}^2/\mathrm{V\,s}$ at $p = 0.01$ GPa to 75.1 $\mathrm{cm}^2/\mathrm{V\,s}$ at $p = 1.01$ GPa. This suggests that the decrease in hole mobility also contributes to the large increase in low-temperature resistivity of $Ce_3Bi_4Pd_3$ at higher pressures.

The increase in energy gap with pressure is also evidenced in magnetoresistance. Figure 4(b) shows the magnetoresistance of $Ce_3Bi_4Pd_3$, $\mathrm{MR} = [\rho(B) - \rho(0)]/\rho(0)$, measured at $T = 10$ K. At low pressures, MR is negative and reaches about -20% at 9 T, in agreement with recent high-field measurements at ambient pressure [21]. With increasing pressure, the MR(B) curves shift continuously upward, reaching about -15% at 9 T for $p = 1.39$ GPa. Our results are in line with the scenario wherein magnetic fields weaken Kondo coupling and therefore suppress the Kondo hybridization gap. At a critical field of $B_c \approx 11$ T, the gap of $Ce_3Bi_4Pd_3$ was argued to collapse to zero temperature in a way consistent with a quantum critical point. For fields higher than B_c, a Fermi-liquid regime is subsequently observed in $\rho(T)$ [21]. Because the insulator-to-metal transition is directly related to the Kondo scale, B_c is naturally expected to increase as the activated gap increases in $Ce_3Bi_4Pd_3$ under pressure. Therefore, at higher pressures, larger magnetic fields would be required to reduce the energy gap, resulting in relatively smaller negative MR with increasing pressure.

In light of our results under hydrostatic pressure, we now turn to the evaluation of the possible ground states of $Ce_3Bi_4Pd_3$. As mentioned earlier, in the WKSM scenario, the reduction in SOC resulting from the substitution of Pt with Pd is argued to be the key tuning parameter that drives the Kondo insulating state in $Ce_3Bi_4Pt_3$ towards the semimetallic state in $Ce_3Bi_4Pd_3$ [19]. However, recent band-structure calculations suggest that the decrease in SOC arising from the nuclear charge difference between Pt and Pd is insufficient to account for the change in the hybridization gap of the two compounds [27]. Instead the difference in the radial extent of the Pt-5d and Pd-4d orbitals is proposed to significantly affect the hybridization between 4f and conduction electrons and thereby the Kondo coupling, despite the substitution being isovolume. These findings are in line with the results from our hydrostatic pressure study and show that the Kondo coupling is the key parameter governing the ground states in $Ce_3Bi_4(Pt/Pd)_3$.

The Kondo coupling strength depends on the hybridization interaction V as $J_K \propto |V|^2/U$, where U is the Coulomb interaction. Our results in $Ce_3Bi_4Pd_3$ suggest that the hybridization interaction scales linearly with pressure leading to the observed quadratic pressure dependence of the energy gap. In the substitution series $Ce_3Bi_4(Pt_{1-x}Pd_x)_3$, the radial extent of the d orbitals plays a similar role to that of applied pressure. Finally, the striking similarities in the evolution of the Kondo insulating gap with magnetic field and applied pressure in $Ce_3Bi_4Pd_3$ [21] and $Ce_3Bi_4Pt_3$ [25,26] provide further evidence for a narrow-gap Kondo insulating ground state in $Ce_3Bi_4Pd_3$.

In summary, we have studied $Ce_3Bi_4Pd_3$ using electrical transport measurements under hydrostatic pressure. At ambient pressure, $Ce_3Bi_4Pd_3$ is a narrow-gap Kondo insulator, evidenced by activated behavior in electrical resistivity and Hall measurements. Under hydrostatic pressure, $Ce_3Bi_4Pd_3$ becomes more insulating, a behavior typical of Kondo insulators such as $Ce_3Bi_4Pt_3$ in the considered pressure range. Moreover, the hybridization gap shows a quadratic increase with pressure akin to the effect of Pt substitution observed in $Ce_3Bi_4(Pt_{1-x}Pd_x)_3$ series. The pressure dependence of carrier density, obtained from Hall resistivity measurements on a microstructure device of $Ce_3Bi_4Pd_3$, as well as the magnetoresistance are in excellent agreement with the increase in energy gap under pressure. Our results suggest that the Kondo coupling prevails as the primary tuning parameter in these materials and $Ce_3Bi_4Pd_3$ is a narrow-gap version of the prototypical Kondo insulator $Ce_3Bi_4Pt_3$.

Methods. Single crystals of $Ce_3Bi_4Pd_3$ were grown by bismuth flux [21] and the combined bismuth-lead flux technique. In the latter, cerium (Ames Lab 99.95%), palladium (99.95%), bismuth (99.999%), and lead (99.999%) were taken in the starting composition Ce : Pd : Bi : Pb = 1 : 1 : 4.25 : 7 in an alumina crucible placed in an evacuated quartz tube and heated to 800 °C in 5 h and kept there for 24 h. The solution was slowly cooled down to 650 °C in 40 h and the excess flux was removed by centrifuging. $Ce_3Bi_4Pd_3$ crystallizes in a cubic structure of space group $I\bar{4}3d$ [40]. The crystallographic structure was verified at room temperature by a Bruker D8 Venture single-crystal diffractometer equipped with Mo radiation. Electrical-resistivity measurements were performed in a standard four-terminal method in which electrical contacts to the samples were made using 12.5-μm platinum wires and silver paste. For samples grown by the Bi-Pb flux (PC3 and PC4), current was applied in the (111) plane, and magnetic field was applied along the [111] direction. For samples grown using the self-flux method (PC1 and PC2), measurements were performed in unoriented samples. The Hall resistivity was measured on a microstructure device fabricated using the focused ion beam (FIB) technique with a scanning electron microscopy (SEM) SCIOS instrument. A single-crystal sample was polished to smaller size ($600 \times 200 \times 20$ $\mu\mathrm{m}^3$), fixed to a sapphire platform (2×2 mm^2), and electrical contacts were made using silver paste and 12.5-μm Pt wires. Micropatterns were directly milled into the above-mentioned sample using Ga ion beam (ion current 65 nA) to fabricate the microstructure device. Electrical-transport measurements under hydrostatic pressure were carried out using a double-layered piston-cylinder-type pressure cell with Daphne 7373 oil as the pressure-transmitting medium. The pressure inside the sample space was determined at low temperatures by the shift of the superconducting transition temperature of a piece of lead

(Pb). Electrical resistivity was measured using an ac resistance bridge (model 372, Lake Shore) at a measuring frequency of 13.7 Hz together with a physical property measurement system (Quantum Design).

Acknowledgments. We acknowledge constructive discussions with Mun K. Chan, Jian-Xin Zhu, and Jan Tomczak. The conception of this work as well the crystal synthesis were supported by the U.S. Department of Energy, Office of Basic Energy Sciences "Science of 100 T" program. M.O.A. acknowledges funding from the Laboratory Directed Research & Development Program. Scanning electron microscope and focused ion beam measurements were supported by the Center for Integrated Nanotechnologies, an Office of Science User Facility operated for the U.S. Department of Energy Office of Science. Measurements under pressure were supported by the U.S. Department of Energy, Office of Basic Energy Sciences "Quantum Fluctuations in Narrow Band Systems" program.

[1] C. L. Kane and E. J. Mele, Z_2 Topological Order and the Quantum Spin Hall Effect, Phys. Rev. Lett. **95**, 146802 (2005).
[2] C. L. Kane and E. J. Mele, Quantum Spin Hall Effect in Graphene, Phys. Rev. Lett. **95**, 226801 (2005).
[3] J. E. Moore and L. Balents, Topological invariants of time-reversal-invariant band structures, Phys. Rev. B **75**, 121306(R) (2007).
[4] R. Roy, Z_2 classification of quantum spin Hall systems: An approach using time-reversal invariance, Phys. Rev. B **79**, 195321 (2009).
[5] M. König, H. Buhmann, L. W. Molenkamp, T. Hughes, C.-X. Liu, X.-L. Qi, and S.-C. Zhang, The quantum spin Hall effect: Theory and experiment, J. Phys. Soc. Jpn. **77**, 031007 (2008).
[6] M. Z. Hasan and C. L. Kane, Colloquium: Topological insulators, Rev. Mod. Phys. **82**, 3045 (2010).
[7] L. Fu, C. L. Kane, and E. J. Mele, Topological Insulators in Three Dimensions, Phys. Rev. Lett. **98**, 106803 (2007).
[8] L. Fu and C. L. Kane, Topological insulators with inversion symmetry, Phys. Rev. B **76**, 045302 (2007).
[9] M. Dzero, J. Xia, V. Galitski, and P. Coleman, Topological Kondo insulators, Annu. Rev. Condens. Matter Phys. **7**, 249 (2016).
[10] X.-L. Qi and S.-C. Zhang, Topological insulators and superconductors, Rev. Mod. Phys. **83**, 1057 (2011).
[11] S. M. Young, S. Zaheer, J. C. Y. Teo, C. L. Kane, E. J. Mele, and A. M. Rappe, Dirac Semimetal in Three Dimensions, Phys. Rev. Lett. **108**, 140405 (2012).
[12] Z. Wang, Y. Sun, X.-Q. Chen, C. Franchini, G. Xu, H. Weng, X. Dai, and Z. Fang, Dirac semimetal and topological phase transitions in A_3Bi (A = Na, K, Rb), Phys. Rev. B **85**, 195320 (2012).
[13] A. A. Burkov, Topological semimetals, Nat. Mater. **15**, 1145 (2016).
[14] B. Q. Lv, T. Qian, and H. Ding, Experimental perspective on three-dimensional topological semimetals, Rev. Mod. Phys. **93**, 025002 (2021).
[15] N. P. Armitage, E. J. Mele, and A. Vishwanath, Weyl and Dirac semimetals in three-dimensional solids, Rev. Mod. Phys. **90**, 015001 (2018).
[16] H.-H. Lai, S. E. Grefe, S. Paschen, and Q. Si, Weyl-Kondo semimetal in heavy-fermion systems, Proc. Natl. Acad. Sci. USA **115**, 93 (2018).
[17] P.-Y. Chang and P. Coleman, Parity-violating hybridization in heavy Weyl semimetals, Phys. Rev. B **97**, 155134 (2018).
[18] C. Cao, G.-X. Zhi, and J.-X. Zhu, From trivial Kondo insulator $Ce_3Pt_3Bi_4$ to topological nodal-line semimetal $Ce_3Pd_3Bi_4$, Phys. Rev. Lett. **124**, 166403 (2020).
[19] S. Dzsaber, L. Prochaska, A. Sidorenko, G. Eguchi, R. Svagera, M. Waas, A. Prokofiev, Q. Si, and S. Paschen, Kondo Insulator to Semimetal Transformation Tuned by Spin-Orbit Coupling, Phys. Rev. Lett. **118**, 246601 (2017).
[20] S. Dzsaber, X. Yan, M. Taupin, G. Eguchi, A. Prokofiev, T. Shiroka, P. Blaha, O. Rubel, S. E. Grefe, H.-H. Lai, Q. Si, and S. Paschen, Giant spontaneous Hall effect in a nonmagnetic Weyl–Kondo semimetal, Proc. Natl. Acad. Sci. USA **118**, e2013386118 (2021).
[21] S. K. Kushwaha, M. K. Chan, J. Park, S. M. Thomas, E. D. Bauer, J. D. Thompson, F. Ronning, P. F. S. Rosa, and N. Harrison, Magnetic field-tuned Fermi liquid in a Kondo insulator, Nat. Commun. **10**, 5487 (2019).
[22] M. F. Hundley, P. C. Canfield, J. D. Thompson, Z. Fisk, and J. M. Lawrence, Hybridization gap in $Ce_3Bi_4Pt_3$, Phys. Rev. B **42**, 6842 (1990).
[23] M. Hundley, P. Canfield, J. Thompson, Z. Fisk, and J. Lawrence, Evidence for a 'coherence' gap in $Ce_3Bi_4Pt_3$, Phys. B: Condens. Matter **171**, 254 (1991).
[24] M. F. Hundley, P. C. Canfield, J. D. Thompson, and Z. Fisk, Substitutional effects on the electronic transport of the Kondo semiconductor $Ce_3Bi_4Pt_3$, Phys. Rev. B **50**, 18142 (1994).
[25] J. C. Cooley, M. C. Aronson, and P. C. Canfield, High pressures and the Kondo gap in $Ce_3Bi_4Pt_3$, Phys. Rev. B **55**, 7533 (1997).
[26] M. Jaime, R. Movshovich, G. R. Stewart, W. P. Beyermann, M. G. Berisso, M. F. Hundley, P. C. Canfield, and J. L. Sarrao, Closing the spin gap in the Kondo insulator $Ce_3Bi_4Pt_3$ at high magnetic fields, Nature (London) **405**, 160 (2000).
[27] J. M. Tomczak, Isoelectronic tuning of heavy fermion systems: Proposal to synthesize $Ce_3Sb_4Pd_3$, Phys. Rev. B **101**, 035116 (2020).
[28] P. S. Riseborough, Theory of the dynamic magnetic response of $Ce_3Bi_4Pt_3$: A heavy-fermion semiconductor, Phys. Rev. B **45**, 13984 (1992).
[29] S. Sen, N. S. Vidhyadhiraja, E. Miranda, V. Dobrosavljević, and W. Ku, Fragility of the Kondo insulating gap against disorder: Relevance to recent puzzles in topological Kondo insulators, Phys. Rev. Res. **2**, 033370 (2020).
[30] M. Pickem, E. Maggio, and J. M. Tomczak, Resistivity saturation in Kondo insulators, Commun. Phys. **4**, 226 (2021).
[31] See Supplemental Material at http://link.aps.org/supplemental/10.1103/PhysRevB.106.L161105 for a discussion on the effect of impurity inclusions on the magnetotransport data.
[32] B. W. Roberts, Survey of superconductive materials and critical evaluation of selected properties, J. Phys. Chem. Ref. Data **5**, 581 (1976).

[33] Y. Imai, F. Nabeshima, T. Yoshinaka, K. Miyatani, R. Kondo, S. Komiya, I. Tsukada, and A. Maeda, Superconductivity at 5.4 K in β-Bi_2Pd, J. Phys. Soc. Jpn. **81**, 113708 (2012).

[34] B. Joshi, A. Thamizhavel, and S. Ramakrishnan, Superconductivity in noncentrosymmetric BiPd, Phys. Rev. B **84**, 064518 (2011).

[35] Y. Li, E. Wang, X. Zhu, and H.-H. Wen, Pressure-induced superconductivity in Bi single crystals, Phys. Rev. B **95**, 024510 (2017).

[36] X. Du, S.-W. Tsai, D. L. Maslov, and A. F. Hebard, Metal-Insulator-Like Behavior in Semimetallic Bismuth and Graphite, Phys. Rev. Lett. **94**, 166601 (2005).

[37] H. T. Chu, P. N. Henriksen, J. Jing, H. Wang, and X. Xu, Magnetic-field dependence of Hall resistance in thin films of pure bismuth, Phys. Rev. B **45**, 11233 (1992).

[38] H. T. Chu, P. N. Henriksen, and J. Alexander, Resistivity and transverse magnetoresistance in ultrathin films of pure bismuth, Phys. Rev. B **37**, 3900 (1988).

[39] M. Lu, R. J. Zieve, J. A. van Hulst, H. M. Jaeger, T. F. Rosenbaum, and S. Radelaar, Low-temperature electrical-transport properties of single-crystal bismuth films under pressure, Phys. Rev. B **53**, 1609 (1996).

[40] W. Hermes, S. Linsinger, R. Mishra, and R. Pöttgen, Structure and properties of $Ce_3Pd_3Bi_4$, CePdBi, and $CePd_2Zn_3$, Monatsh. Chem. **139**, 1143 (2008).